Forecasting Changes in Urban Heat Island in the US Southwest

Daniel Burillo[1*]
Research Associate
daniel.burillo@asu.edu

Mikhail V. Chester[1]
Assistant Professor
mchester@asu.edu

Andrew Chang[2]
Software Engineer
andrewjc@google.com

David Thau[2]
Manager of Developer Relations
thau@google.com

[1]Department of Civil, Environmental and Sustainable Engineering, Arizona State University
[2]Google Earth Engine and Google Earth Outreach, Google

* Author to whom correspondence should be addressed

Report No. ASU-SSEBE-CESEM-2015-RPR-004
September 2015
https://repository.asu.edu/items/35352

Introduction

Recent developments in computational software and public accessibility of gridded climatological data have enabled researchers to study Urban Heat Island (UHI) effects more systematically and at a higher spatial resolution. Previous studies have analyzed UHI and identified significant contributors at the regional level for cities, within the topology of urban canyons, and for different construction materials [1][2][3]. In UHIs, air is heated by the convective energy transfer from land surface materials and anthropogenic activities. Convection is dependent upon the temperature of the surface, temperature of the air, wind speed, and relative humidity. At the same time, air temperature is also influenced by greenhouse gases (GHG) in the atmosphere. Climatologists project a 1-5°C increase in near-surface air temperature over the next several decades [4], and 1-4°C specifically for Los Angeles and Maricopa during summertime due to GHG effects [5][6]. With higher ambient air temperatures, we seek to understand how convection will change in cities and to what ends. In this paper we develop a spatially explicit methodology for quantifying UHI by estimating the daily convection thermal energy transfer from land to air using publically available gridded climatological data, and estimate how much additional energy will be retained due to lack of convective cooling in scenarios of higher ambient air temperature.

Methodology

Governing Equations

To estimate convection throughout cities, we compute the thermal transfer rate geospatially using the Google Earth Engine API. All variables are defined in the Notation section at the end.

$$q_{conv} = h\left(T_{sur} - T_{sky}\right) \qquad \text{W m}^{-2} \qquad (1)$$

Convection is a function of a thermal difference between two mediums (T_{sur} - T_{sky}) and an energy transfer coefficient (h). Temperature values used for land surface and air are based on data obtained from the MODIS satellite and Daymet Climatological summaries respectively as described in the Data subsection. The heat transfer coefficient equation that we use assumes laminar flow over a flat plate [3], and a constant characteristic surface length of L=0.5, whereby convection is calculated uniformly per unit land area regardless of topology.

$$h = 0.664\ (k\ Pr^{0.3}\ v^{-0.5} L^{-0.5}\ U^{0.5}) \qquad \text{W m}^{-2}\ \text{C}^{-1} \qquad (2)$$

The heat transfer coefficient is computed based on thermophysical properties of air, which we base on available data for wind speed, air temperature, and relative humidity. Wind speed is directly obtained from Gridmet climatological summaries, air temperature is the same T_{sky} value as previous, and relative humidity (RH) values are based on Gridmet as described in the Data subsection. The remaining equations for the thermophysical properties of air are approximated based on previous research in which air properties were fit to polynomial expressions for standard barometric pressure conditions of 101.3 kPa with coefficients of determination all >0.9999 using the constant values listed in Table 1 [7]. The citation provided explicit equations

for air property values where *RH*=0%, several sample point values at *RH*=50%, and graphical compilations of results. The equations used in our methods below are approximated based on those equations and validated numerically within 0.9999 of the provided sample points.

$$k = SK_0 + SK_1\, t + \left(SK_2\, t^2 + SK_3\, t^3 + SK_4\, t^4\right) RH \qquad \text{W m}^{-1}\,\text{C}^{-1} \qquad (3)$$

$$Pr = SP_0 + \left(SP_1\, t + SP_2\, t^2 + SP_3\, t^3 + SP_4\, t^4\right)(1.02\, RH - 0.02) \qquad \text{dimensionless} \qquad (4)$$

$$v = {}^{\mu}/_{\rho} \qquad \text{m}^2\,\text{s}^{-1} \qquad (5)$$

$$\mu = SV_0 + SV_1\, t + \left(SV_2\, t^2 + SV_3\, t^3 + SV_4\, t^4\right) RH \qquad \text{kg m}^{-1}\,\text{s}^{-1} \qquad (6)$$

$$\rho = SD_0 + SD_1\, t + SD_2\, t^2 + SD_3\, t^3\,(0.705\, RH + 0.295) \qquad \text{kg m}^{-3} \qquad (7)$$

Table 1 Numerical constants for polynomial fit expressions for air thermal conductivity, Prandtl number, dynamic viscosity, and density used in the calculation of the convective heat transfer coefficient. [7]

k - Thermal conductivity ($W\ m^{-1}\ C^{-1}$)	Pr - Prandtl number (dimensionless)	μ - Dynamic viscosity ($kg\ m^{-1}\ s^{-1}$)	ρ - Density ($kg\ m^{-3}$)
SK_0 = 2.40073953E-02	SP_0 = 7.215798365E-01	SV_0 = 1.715747771E-05	SD_0 = 1.293393662
SK_1 = 7.278410162E-05	SP_1 = -3.703124976E-04	SV_1 = 4.722402075E-08	SD_1 = -5.538444326E-03
SK_2 = -1.788037411E-07	SP_2 = 2.240599044E-05	SV_2 = -3.663027156E-10	SD_2 = 3.860201577E-05
SK_3 = -1.351703529E-09	SP_3 = -4.162785412E-07	SV_3 = 1.873236686E-12	SD_3 = -5.2536065E-07
SK_4 = -3.322412767E-11	SP_4 = 4.969218948E-09	SV_4 = -8.050218737E-14	

Data

Tool Used

Data are accessed and processed using the publically available Google Earth Engine (GEE) tool, wherein the Advanced Programmer Interface (API) “Reducer” and “ReduceRegions” functions are used to average daily records at 200m resolution within the county regions for the analysis periods [8]. MODIS and Daymet data sets are recorded at native resolutions of approximately 1km x 1km and Gridmet 2km x 2km. None of these data sets, nor the boundaries of the analysis regions, are in perfect alignment for data intersection. Therefore a smaller data processing resolution of 200m was chosen to ensure reasonable intersection of sample data in calculating convection without exceeding time and memory constraints in computational processing.

Geographic Regions

USA 2010 census geography files are used to clip the gridded climatological data to the Los Angeles and Maricopa County regions [9]. Los Angeles and Maricopa counties are large regions in the desert southwest at approximately 13,000 km^2 and 24,000 km^2 of land surface area respectively. Both of these regions are located in the United States’ desert southwest. The desert southwest is known for its particularly hot summers and rapid urban development, which make it an interesting region to study UHI, the effects of increased air temperatures, and

potential for UHI mitigation strategies. LA and Maricopa include a broad mix of landscapes from the beach near the Pacific Ocean, to urban developed areas, rural lands, rivers, forests, agriculture, flat desert, and rocky mountainous deserts.

Climatological Inputs

The mean of daily source records for climatological values are used for the period June, July, and August (JJA) of 2010 as inputs to the governing equations. This period was chosen to represent the average for the hottest period of the most current year with complete data availability from the three sources. Table 2 shows a statistical summary of the inputs for each county and the primary source data, where T_{sur}, T_{sky}, and RH are the spatially explicit means of the daily daytime and nighttime values, and minimum and maximum values as recorded in the source respectively.

Across both counties, high daytime LST values are in pavement-dense urban areas as well as rocky desert, and low values are in more wet areas for both counties, including: forest, agriculture, rivers, and near the beach [10][11][12]. High nighttime LST values are predominantly in more dense urban areas. Sky temperature records are for measurements at 2 meters above ground level. Maximum sky temperatures are in the desert regions and central urban developed areas, and minimums are near the areas with significant water and dense vegetation [13]. Wind speed records are for measurements 10 meters above ground level. Average wind speed is highest in the large open desert areas, and lowest in the central downtown valleys [14]. Humidity is highest in LA near the ocean and lowest in the northeastern desert, whereas in Maricopa, humidity is highest outside the city and lowest in the urban developed area [14].

Table 2 Statistical summary of source data and values used in calculation of convection for 2010 JJA period.

2010 JJA Average	T_{sur} (°C)	T_{sky} (°C)	U (m/s)	RH (%)	T_{sur_day} (°C)	T_{sur_night} (°C)	T_{sky_max} (°C)	T_{sky_min} (°C)	RH_{max} (%)	RH_{min} (%)
LA										
min	16.1	11.5	1.7	31.8	21.6	5.7	16.0	4.2	44.5	17.1
max	35.2	25.0	5.7	80.1	54.9	18.1	33.2	16.8	100.0	66.7
mean	27.8	20.6	3.1	55.2	41.0	14.5	27.0	14.3	78.5	32.0
std dev	3.5	2.2	1.0	11.8	6.6	1.4	3.3	1.6	14.1	10.9
Maricopa										
min	24.6	17.7	2.5	19.1	31.3	13.8	24.1	11.3	28.7	9.1
max	41.7	30.5	5.1	31.1	60.6	26.2	39.7	21.8	49.9	15.2
mean	36.9	28.5	3.3	23.9	53.6	20.2	37.1	19.8	37.0	10.8
std dev	2.2	1.7	0.5	2.5	4.0	1.8	2.0	1.6	4.6	0.7

Convection Forecasting

Convection is calculated using the governing equations at each spatial location in each county with source data for JJA 2010, and then again by adding 1-4°C to the mean sky temperature, T_{sky}, for a total of five scenarios. The statistical distribution of convection rates is compared in each scenario, and convection heat maps are produced to analyze the trends within and across each county.

Results

The average daily convection was 32 and 65 TWh in JJA 2010 LA and Maricopa counties respectively, and would have been almost half of that at 18 and 37 TWh if ambient air temperatures were 4°C higher. Each 1°C increase in ambient air temperature results in an average 11% decrease in convection air cooling of the land surface by heat transfer in these regions in the summertime. Figure 1 shows convection rates spatially at a 1km x 1km resolution and statistical summary for each county in each scenario.

Maricopa has a wider range and less variation in its convection rates than LA. Maricopa's lowest convection rate is -48 W/m^2, coincident with agricultural lands where the average daily air temperature is 3°C higher than LST. This is most clearly visible in Figure 1 in the large blue shaded areas along the Gila River, and the same is true to a lesser magnitude for the smaller patches of agriculture and rivers along the outskirts of the Phoenix metropolitan area. LA's lowest convection rate is -10 W/m^2 coincident with regions where the average air temperature is up to 1°C higher than the average land surface temperature in the Angeles National Forest, Santa Monica Mountains, Green Valley, nearby small bodies of water, and patches of agricultural lands in the northern Mojave Desert region of the county. The maximum convection rates for both counties is similar at 210 and 190 W/m^2 for LA and Maricopa respectively and occurs outside of cities in desert regions. These are the places with the highest temperature difference between day and night and minimum and maximum. LA has more variance in its convection with a standard deviation of 38 W/m^2 compared to Maricopa's 27 W/m^2 coincident with its larger diversity of land and climates types including large forests, valleys, desert, and near-ocean lands.

Within the urban areas of each county, convection rates are generally higher than average. The low convection rate exceptions are in areas with significant water and vegetation including in LA: Woodley Park, Blair Hills, Whittier Narrows, and in Maricopa: the Ingleside club, Chaparral Park, Garden Lakes Estates, and McCormick Ranch. Convection rates in urban areas are generally higher further from these high water and vegetation areas.

q_{conv} 2010 JJA (W/m^2)

	LA	Maricopa
min	-9.7	-48.2
max	210.1	188.8
mean	102.2	112.0
std dev	38.3	26.5

q_{conv} 2010 JJA +1°C (W/m^2)

	LA	Maricopa
min	-21.8	-63.2
max	197.5	176.1
mean	91.5	100.6
std dev	38.6	26.6

q_{conv} 2010 JJA +2°C (W/m^2)

	LA	Maricopa
min	-37.9	-79.2
max	184.5	163.1
mean	80.5	88.8
std dev	39.3	26.8

q_{conv} 2010 JJA +3°C (W/m^2)

	LA	Maricopa
min	-58.0	-96.4
max	171.1	149.9
mean	68.9	76.7
std dev	40.6	27.1

q_{conv} 2010 JJA +4°C (W/m^2)

	LA	Maricopa
min	-82.0	-115.2
max	157.0	136.4
mean	56.8	64.1
std dev	43.0	27.5

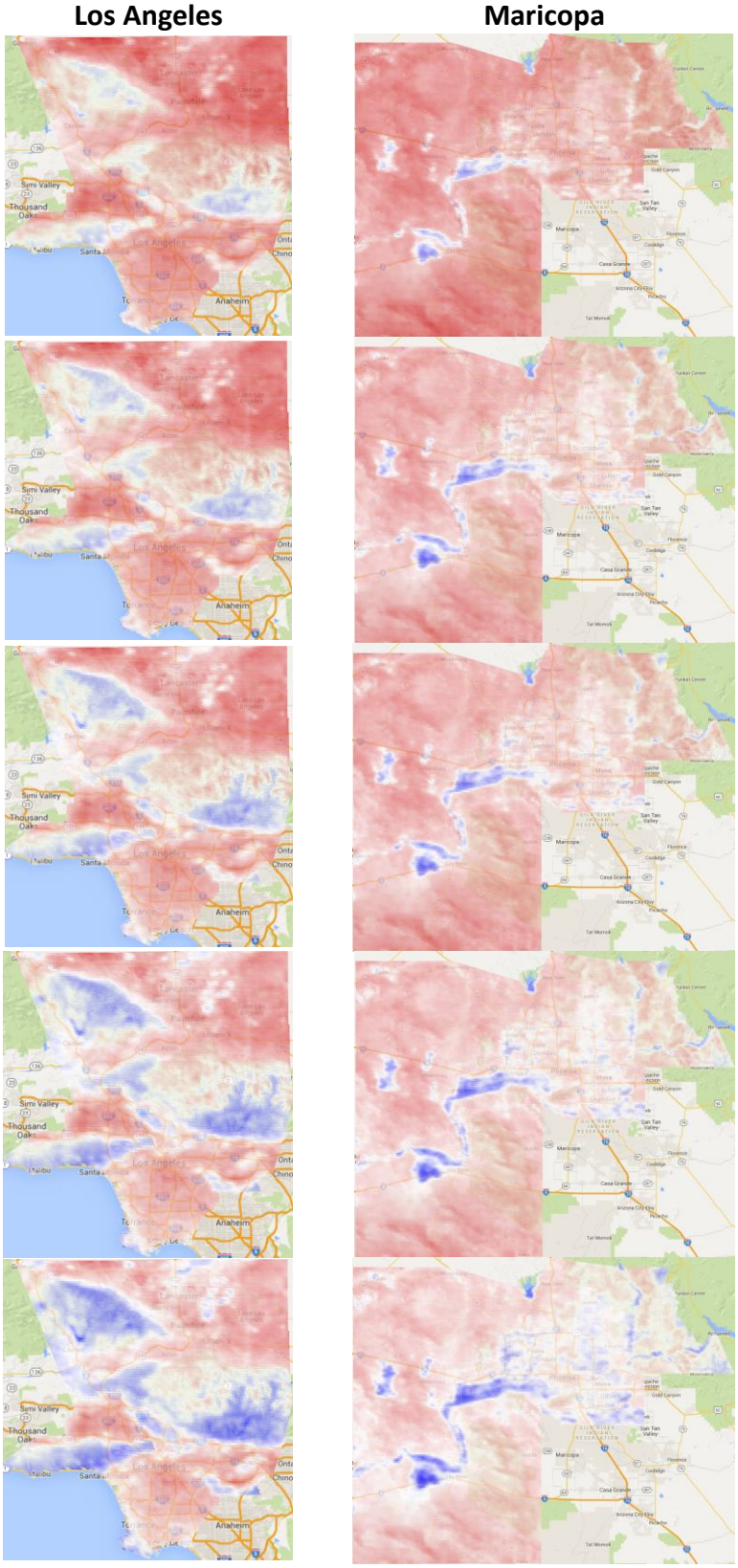

Figure 1 Maps of convection in LA and Maricopa Counties for JJA 2010 and ambient air temperature projected scenarios +1 to 4°C. Color shadings range from -115 W/m^2 minimum in blue to 210 W/m^2 maximum in red.

Uncertainty

The accuracy of the results are limited to the accuracy of the input data, which are mostly an average of two daily points. The LST values used are daytime and nighttime averages, which were recorded at average local solar times of 5:20 PM and 2:00AM for day and night in LA respectively, and 5:30 PM and 4:15 AM in Maricopa respectively. The sky temperature and relative humidity values used are the average of the daily maximum and minimum records. If the daytime and nighttime LST values are equal to the maximum and minimum LST and the distributions of LST, air temperature, and humidity are the same throughout the 24-hour diurnal cycle, then our method produces accurate average estimates. If that is not the case, and the distributions are skewed differently, then results may be skewed as well. This uncertainty could be significantly reduced and this research advanced by using hourly climatological data to more accurately estimate convection on an hourly basis instead of a daily basis. Our equations also assume a constant standard barometric pressure, which could also be more accurately accounted for as an input variable using hourly data as well.

Discussion

Urban planners and policy makers in LA, Maricopa, and other developing desert regions, may consider this research insightful in balancing competing priorities for UHI effects, agriculture, and water resource availability. Increased ambient air temperature expects reduced convection and therefore increased thermal energy retention in the land surface by about 11% per 1°C. Extreme heat events impact peak electric demand at a rate of 1.5 – 2% per 0.6°C due to increased demand for building cooling services [15], and cardiovascular illness mortalities at rate of 2.6% per 4.7°C [16]. To counter UHI, we find that negative convection occurs on heavily watered and vegetated lands wherein irrigation effectively provides a cooling effect in and around cities. Thus, a solution may appear simple to mix urban development with agriculture and reduce UHI effects, but water is not a free or infinite resource and land-use zoning is a complex dynamic process [17]. California is experiencing drought [18], Arizona will likely have significantly less water supply than in previous years from the Colorado River [19], and continued urban growth means that cities will likely experience insufficient streamflow for all of their desired ecological processes [20]. All of these issues are important in regional governance, which further emphasizes the significance of high quality spatial data and cloud computing tools that enable researchers to continue to provide better insight into the dynamics of complex social-ecological and technical systems.

Notation

Symbol	Units	Description
q_{conv}	W m^{-2}	Convection heat transfer
h	W m^{-2} °C^{-1}	Convective heat transfer coefficient
T_{sur}	°C	Average land surface temperature
T_{sur_day}	°C	Daytime land surface temperature
T_{sur_night}	°C	Night time Land surface temperature
T_{sky}	°C	Average air temperature
T_{sky_max}	°C	Maximum air temperature
T_{sky_min}	°C	Minimum air temperature
t	°C	Average air temperature (equal to T_{sky})
RH	%	Average relative humidity
RH_{max}	%	Maximum relative humidity
RH_{min}	%	Minimum relative humidity
k	W m^{-1} °C^{-1}	Air thermal conductivity
Pr	dimensionless	Prandtl number
v	m^2 s^{-1}	Kinematic viscosity of air
L	m	Characteristic length of surface
U	m s^{-1}	Wind speed
μ	kg m^{-1} s^{-1}	Dynamic viscosity of air
ρ	kg m^{-3}	Density of air

References

[1] L. Zhao, X. Lee, R. B. Smith, and K. Oleson, "Strong contributions of local background climate to urban heat islands," *Nature*, vol. 511, no. 7508, pp. 216–219, 2014.

[2] M. a. Hart and D. J. Sailor, "Quantifying the influence of land-use and surface characteristics on spatial variability in the urban heat island," *Theor. Appl. Climatol.*, vol. 95, no. 3–4, pp. 397–406, 2009.

[3] J. Gui and P. Phelan, "Impact of pavement thermophysical properties on surface temperatures," *J. Mater. …*, vol. 19, no. August, 2007, pp. 683–690, 2007.

[4] Intergovernmental Panel on Climate Change, "Summary for policymakers," *Clim. Chang. 2014 Mitig. Clim. Chang. Contrib. Work. Gr. III to Fifth Assess. Rep. Intergov. Panel Clim. Chang.*, pp. 1–31, 2014.

[5] A. Hall, F. Sun, D. Walton, S. Capps, X. Qu, H.-Y. Huang, N. Berg, A. Jousse, M. Schwartz, M. Nakamura, and R. Cerezo-Mota, "Mid-Century Warming in the Los Angeles Region," vol. 1, no. 33, 2012.

[6] M. Georgescu, M. Moustaoui, a. Mahalov, and J. Dudhia, "Summer-time climate impacts of projected megapolitan expansion in Arizona," *Nat. Clim. Chang.*, vol. 3, no. 1, pp. 37–41, 2012.

[7] P. T. Tsilingiris, "Thermophysical and transport properties of humid air at temperature range between 0 and 100 °C," *Energy Convers. Manag.*, vol. 49, no. 5, pp. 1098–1110, 2008.

[8] "Google Earth Engine: A Planetary-scale Platform for Environmental Data & Analysis," 2012. [Online]. Available: https://earthengine.google.org/. [Accessed: 01-May-2015].

[9] G. US Census Bureau, "TIGERweb County-Based Data Files 2010 Census."

[10] "MODIS/Aqua Land Surface Temperature and Emissivity Daily L3 Global 1 Km Grid SIN.," *Land Processing Distributed Active Archive Center. United States Geological Survey*, 2014. [Online]. Available: https://lpdaac.usgs.gov/products/modis_products_table/myd11a1. [Accessed: 20-Oct-2014].

[11] Z. Wan, "MODIS LST Products Users' Guide," *University of California, Santa Barbara*, 2013. [Online]. Available: http://www.icess.ucsb.edu/modis/LstUsrGuide/usrguide_1dtil.html#alg. [Accessed: 20-Oct-2014].

[12] M. a. Friedl, D. Sulla-Menashe, B. Tan, A. Schneider, N. Ramankutty, A. Sibley, and X. Huang, "MODIS Collection 5 global land cover: Algorithm refinements and characterization of new datasets," *Remote Sens. Environ.*, vol. 114, no. 1, pp. 168–182, 2010.

[13] P. E. Thornton, M. M. Thornton, B. W. Mayer, N. Wilhelmi, Y. Wei, and R. B. Cook, "Daily surface weater on a 1 km grid for North America, 1980-2012." Oak Ridge National Laboratory Distributed Active Archive Center, Oak Ridge, Tennessee, 2012.

[14] J. T. Abatzoglou, "Development of gridded surface meteorological data for ecological applications and modelling," *Int. J. Climatol.*, vol. 33, no. 1, pp. 121–131, 2013.

[15] H. Akbari, "Energy Saving Potentials and Air Quality Benefits of," in *First International Conference on Passive and LowEnergy Cooling for the Built Environment, Athens, Greece, May 17-24,2005*, 2005, pp. 1–19.

[16] R. Basu and B. D. Ostro, "A multicounty analysis identifying the populations vulnerable to mortality associated with high ambient temperature in California.," *Am. J. Epidemiol.*, vol. 168, no. 6, pp. 632–7, Sep. 2008.

[17] A. H. Whittemore, "How the Federal Government Zoned America: The Federal Housing Administration and Zoning," *J. Urban Hist.*, vol. 39, no. 4, pp. 620–642, 2013.

[18] M. E. Mann and P. H. Gleick, "Climate change and California drought in the 21st century," *Proc. Natl. Acad. Sci.*, vol. 112, no. 13, p. 201503667, 2015.

[19] N. S. Christensen, A. W. Wood, N. Voisin, D. P. Lettenmaier, and R. N. Palmer, "The Effects of Climate Change on the Hydrology and Water Resources of the Colorado River Basin," *Clim. Chang.*, no. Figure 1, pp. 337–363, 2004.

[20] R. I. McDonald, P. Green, D. Balk, B. M. Fekete, C. Revenga, M. Todd, and M. Montgomery, "Urban growth, climate change, and freshwater availability.," *Proc. Natl. Acad. Sci. U. S. A.*, vol. 108, no. 15, pp. 6312–6317, 2011.